Arch Appl Mech
DOI 10.1007/s00419-012-0714-5

ORIGINAL

Konstantinos V. Spiliopoulos · Nikos G. Dais

A powerful force-based approach for the limit analysis of three-dimensional frames

Received: 22 April 2012 / Accepted: 30 October 2012

Abstract For the estimation of the strength of a structure, one could avoid detailed elastoplastic analysis and resort, instead, to direct limit analysis methods that are formulated within linear programming. This work describes the application of the force method to the limit analysis of three-dimensional frames. For the limit analysis of a framed structure, the force method, being an equilibrium-based approach, is better suited than the displacement method and results, generally, to faster solutions. Nevertheless, the latter has been used mostly, since it has a better potential for automation. The difficulty for the direct computerization of the force method is to automatically pick up the structure's redundant forces. Graph theory concepts may be used to accomplish this task, and a numerical procedure was proposed for the optimal plastic design of plane frames. An analogous approach is developed herein for the limit analysis of space frames which is computationally more cumbersome than the limit analysis of plane frames. The proposed procedure results in hypersparse matrices, and in conjunction with the kinematic upper bound linear program which is solved by a sparse solver, the proposed method appears computationally very efficient. It is also proved that it is much more effective than any displacement-based formulation. The robustness and efficiency of the approach are testified by numerical examples for grillages and multi-storey frames that are included.

Keywords Numerical methods, Limit analysis, Force method, Graph theory, Grillages, Multi-storeyed frames

1 Introduction

In order to establish safety and integrity for a structure made of an elastoplastic material, an engineer has to determine its strength as well as its ductility. The computational approach, which is most often used to accomplish this, is the step-by-step analysis. This analysis is formulated using the direct stiffness approach which is based on the displacement method. This approach is quite cumbersome as one has to follow in an incremental way the load history taking into account the continuous plastic stressing and possible plastic unstressing by continuously re-formulating and re-decomposing the stiffness matrix.

The three-dimensional character of a space frame increases the complexity of the approach, and thus, published results on the step-by-step analysis of space frames are much rarer than those for plane frames. Among these one could mention [1–3]. In these works second-order effects are included, and plasticity is simulated as concentrated plastic hinges of zero length of a material having rigid plastic behavior. In a recent publication [4] strain hardening effects are taken into account.

When common civil engineering structures are subjected to monotonic loading, their limit load provides the threshold above which the deformations start to get large [5]. Then, there is no need to calculate the

K. V. Spiliopoulos (✉) · N. G. Dais
Department of Civil Engineering, Institute of Structural Analysis and Antiseismic Research,
National Technical University of Athens, Zografou, 157-80 Athens, Greece
E-mail: kvspilio@central.ntua.gr

Published online: 18 November 2012

deformations prior to collapse, which could be estimated through a step-by-step analysis, and one may resort to an alternative way of evaluating the limit load. This is provided by the upper and lower bound theorems of plasticity, and the numerical methods that are used are called direct methods of limit analysis. A natural framework to formulate a direct method for the limit analysis problem is linear programming (LP). In this way the deficiencies of the incremental method are avoided, and one seeks for the value of the limit load right from the start of the calculations.

Although the formulation of limit analysis as an LP problem goes back to the early seventies [6], it always remains a timely approach, due to the continuous development of optimization algorithms, considered for its solution, that help us to solve increasingly large-size problems [7]. There is a big evolution in these algorithms starting from the standard simplex method [8], later the less-expensive revised simplex method, up to the interior-point algorithms, which were initiated by [9]. Many publications have appeared in recent literature using interior points; see, for example, two representative articles: a two-dimensional structural [10] and a geotechnical mechanics [11] problem. Also taking into account the sparsity of the matrices involved has a big impact on the amount of the computer time spent for the solution [12]. Thus, formulations concerning specific limit analysis problems [13] are continuously adapted to comply with the advances in all the fields of numerical analysis.

In relation to frames, a computer program with the name CEPAO [14] was written, which used LP for the limit and shakedown load evaluation of 2D frames; recently, this program was extended to the case of the limit analysis [15] and the design of 3D frames [16]. The procedures are built within the displacement method of description, and the LP problem is solved with the aid of the simplex technique. Using also the displacement description, an interior-point algorithm was recently employed for the limit analysis of space frames [17].

In all the aforementioned works, plastic hinges are almost exclusively used to model the plastic effects. The reason for the popularity of the plastic hinge model stems from the fact that it provides a computationally quick way to assess the inelastic behavior of the structure. According to this model, plastic effects are considered lumped at some predefined cross sections. Additionally, one does not have to consider a detailed stress description over the cross section but may get their overall behavior in the form of the generalized forces (forces and moments on the cross section). The section is fully plasticized whenever the combination of these forces touches a yield surface called an interaction surface. These surfaces can be determined for steel frames from the plastic capacities of a given cross section. On the other hand, interaction surfaces for reinforced concrete frames may be determined from the amount of reinforcement [18]. Sufficient ductility capacities, so as to allow for redistribution of forces, for both types of frames are assumed to hold.

Coming now to the formulation of the limit analysis problem, we have to note that equilibrium is a more important condition than compatibility, and therefore, the alternative description of the frame, which is the force method, is better suited. Using this description, for a statically indeterminate frame, equilibrium equations must be established between the unknown hyperstatic forces as well as with the applied loading. The reason that, even in limit analysis, the displacement method is much more in use than the force method is that it may be automated more easily. One may get, however, an indirect access to the formulation by the force method from its displacement counterpart, using the so-called algebraic approach. Such a methodology [19], which in the context of limit analysis was proposed in [20], involves a degree of approximation and generally produces dense matrices.

In [21] one may find a classification of different ways that may lead to the force method, among which is the class of the topological approaches which may be used to get a direct formulation. These are based on the topological view of a frame as a directed graph. Thus, concepts from graph theory like a minimum path technique and a cycle basis may be utilized.

In the present work a topological approach forms a part of a novel direct method which, utilizing a plastic hinge model of zero length, addresses the problem of the limit analysis of space frames using the upper bound theorem of plasticity, assuming first-order theory. The method adjusts an algorithm [22] that was used for plane frames [22–24] to establish equilibrium with the hyperstatic forces of a space frame. The algorithm is based on the repeated use of the minimum path-finding technique of the graph theory so as to establish the shortest path between the two ends of members of the frame going around the structure. The minimum path between the points of application of each load forms a cantilever in space which is used to satisfy equilibrium with the applied loads. The proposed way is shown to lead to the formulation of a LP program with highly sparse matrices whose solution requires the least amount of computing time, as compared to any displacement-based LP which is almost exclusively currently used.

Examples of application for various types of space frames like grillages and 3D buildings show the robustness and computational efficiency of the proposed method. Although the examples considered are for steel frames, one may equally apply the method, as already discussed, to reinforced concrete frames of sufficient ductility capacity.

2 General considerations

A typical 3D-framed structure is shown in Fig. 1. One may also see some numbering of the nodes, which mark the beginning and the end of each member, thus showing the direction of the member. One may assume an additional node (node 10 in Fig. 1) and additional "ground" members, which connect this node with the foundation nodes, to portray ground support.

The whole frame may thus be represented by a closed 3D directed graph. Any such graph can be topologically embedded into a 2D polyhedron [25], whose diagrammatic form may be seen in Fig. 2.

Let us suppose that the structure is subjected to proportional loading. Using entirely equilibrium arguments, one may write the following equation:

$$\mathbf{Q}_{\mathrm{N}} = \mathbf{B} \cdot \mathbf{p} + \mathbf{B}_0 \cdot \mathrm{s} \tag{1}$$

where $\mathbf{Q}_{\mathrm{N}}$ are the independent generalized forces of the structure along the global axes whose positive directions are shown in Fig. 1.

The first term of (1) is due to the indeterminacy of the frame with $\mathbf{p}$ being the vector of the unknown forces and $\mathbf{B}$ the corresponding equilibrium rectangular matrix, whereas the second term comes from the equilibrium with the applied loads with s being the proportional load factor and $\mathbf{B}_0$ the corresponding equilibrium column vector.

For a typical member i of the framed structure, these stress resultants are given in its local axes *{1, 2, 3}*, by $\bar{\mathbf{Q}}_{\mathrm{N}}^{(\mathrm{i})} = \{\mathrm{F}_{1,\mathrm{j}}, \mathrm{F}_{2,\mathrm{j}}, \mathrm{F}_{3,\mathrm{j}}, \mathrm{M}_{1,\mathrm{j}}, \mathrm{M}_{2,\mathrm{j}}, \mathrm{M}_{3,\mathrm{j}}\}^{(\mathrm{i})}$ that correspond to the axial force, the two shear forces, the twisting moment, and the two bending moments at its starting end j.

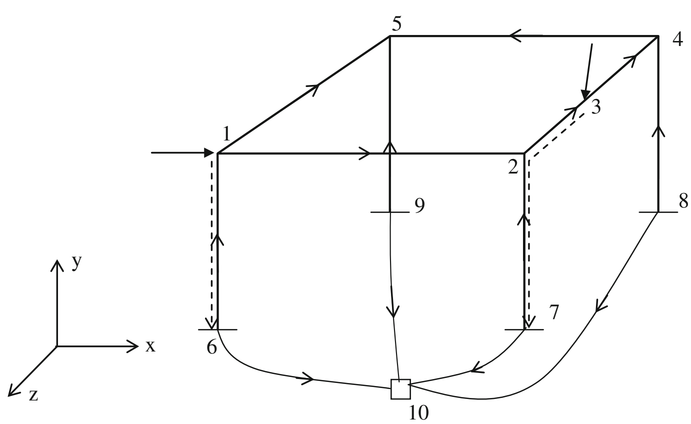

Fig. 1 Typical space frame with ground node

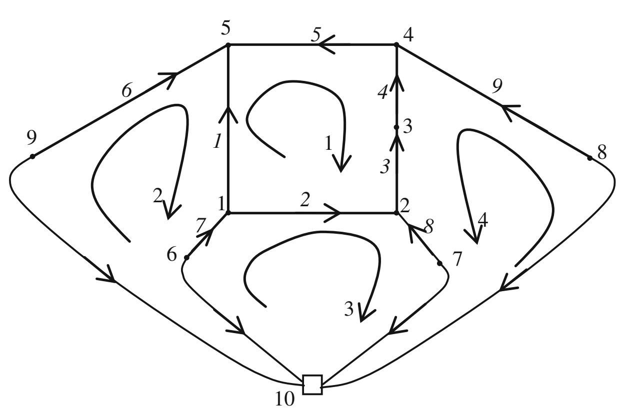

Fig. 2 Graph representation of original structure, node and member numbering, cycle basis and cycle numbering

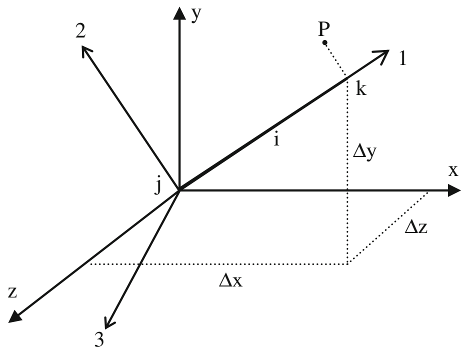

Fig. 3 Resolution to local axes

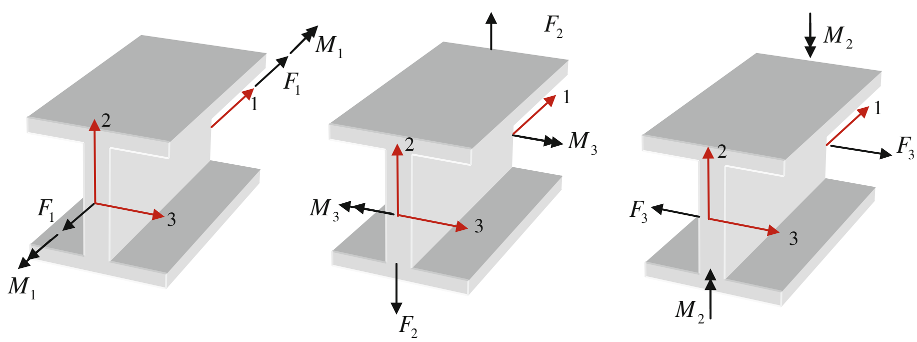

Fig. 4 Positive axial, shear, torsional, and bending moments at the two ends of a member

The local axes form an orthogonal set with the direction of axis *1* coinciding with the direction of the member (Fig. 3). An arbitrary point P must now be used to define the local axis *2*. One good choice could be for this point to lie on one of the principal axes of the cross section. The local axis *2* may be formed as lying in the plane defined from this point and the local axis *1*. Local axis *3* is then uniquely defined as perpendicular to this plane.

If we satisfy equilibrium along the element, we may find the corresponding forces and moments at its finishing end k. Thus, by grouping the forces and moments at the two ends, one may write:

$$\bar{\mathbf{Q}}_{(\mathrm{i})} = \mathbf{T}^{\mathrm{T}}_{(\mathrm{i})} \cdot \bar{\mathbf{Q}}^{(\mathrm{i})}_{\mathrm{N}} \tag{2}$$

where the superscript "T" denotes the transpose of a matrix or a vector.

The matrix $\mathbf{T}_{(\mathrm{i})}$ is given by:

$$\mathbf{T}_{(\mathrm{i})} = [\mathbf{I}_6 \mid \mathbf{E}]^{(\mathrm{i})} \tag{3}$$

with $\mathbf{E} = \left[\begin{array}{ccc:c} & \mathbf{I}_3 & & \mathbf{0}_3 \\ \hdashline 0 & 0 & 0 & \\ 0 & 0 & -\mathrm{L} & \mathbf{I}_3 \\ 0 & -\mathrm{L} & 0 & \end{array}\right]$, $\mathbf{I}_6$ being the 6×6 unit matrix, $\mathbf{I}_3$ and $\mathbf{0}_3$ the 3×3 unit and zero matrices, respectively, and L the length of the member i.

The assumed sign convention for positive forces and moments along the local axes 1, 2, 3 at the two ends of a member may be seen in Fig. 4.

Thus, one may now write for the whole structure:

$$\bar{\mathbf{Q}} = \mathbf{T}^{\mathrm{T}} \cdot \bar{\mathbf{Q}}_{\mathrm{N}} \tag{4}$$

with $\mathbf{T}$ being constructed from the individual elements.

Next, one may establish a transformation of the global stress resultants to the local ones at the starting end j of the member i (Fig. 3). This may be accomplished through the unit vectors along the three axes which are related through their vector products. It may be found that:

$$\bar{\mathbf{Q}}_{\mathrm{N}} = \boldsymbol{\Lambda} \cdot \mathbf{Q}_{\mathrm{N}} \tag{5}$$

The matrix $\boldsymbol{\Lambda}$ may now be constructed from each individual element $\boldsymbol{\Lambda}_{(\mathrm{i})} = \left[\begin{array}{c:c} \boldsymbol{\Lambda}'_{(\mathrm{i})} & \mathbf{0}_3 \\ \hdashline \mathbf{0}_3 & \boldsymbol{\Lambda}'_{(\mathrm{i})} \end{array}\right]$ with:

$$\boldsymbol{\Lambda}_{(\mathrm{i})} = \left[\begin{array}{c:c:c} \frac{\Delta x}{L} & \frac{\Delta y}{L} & \frac{\Delta z}{L} \\ \hdashline \frac{B}{R}\cdot\frac{\Delta z}{L} - \frac{C}{R}\cdot\frac{\Delta y}{L} & -\frac{A}{R}\cdot\frac{\Delta z}{L} + \frac{C}{R}\cdot\frac{\Delta x}{L} & \frac{A}{R}\cdot\frac{\Delta y}{L} - \frac{B}{R}\cdot\frac{\Delta x}{L} \\ \hdashline \frac{A}{R} & \frac{B}{R} & \frac{C}{R} \end{array}\right]^{(\mathrm{i})} \tag{6}$$

with the following definitions:

$$\begin{aligned} A &= \frac{\Delta y}{L} \cdot \Delta z_P - \frac{\Delta z}{L} \cdot \Delta y_P, \\ B &= -\frac{\Delta x}{L} \cdot \Delta z_P + \frac{\Delta z}{L} \cdot \Delta x_P, \\ C &= \frac{\Delta x}{L} \cdot \Delta y_P - \frac{\Delta y}{L} \cdot \Delta x_P, \\ R &= \sqrt{A^2 + B^2 + C^2} \end{aligned}$$

where

$$\begin{aligned} &\Delta x_P = x_P - x_j, \quad \Delta y_P = y_P - y_j, \quad \Delta z_P = z_P - z_j \\ &\Delta x = x_k - x_j, \quad \Delta y = y_k - y_j, \quad \Delta z = z_k - z_j \end{aligned}$$

with the above entities denoting the x, y and z coordinates of P and of the ends j and k of the element i.

By combining (1) and (5) one may write:

$$\bar{\mathbf{Q}}_{\mathrm{N}} = \mathbf{G} \cdot \mathbf{p} + \mathbf{g}_0 \cdot \mathrm{s} \tag{7}$$

where $\mathbf{G} = \boldsymbol{\Lambda} \cdot \mathbf{B}$ and $\mathbf{g}_0 = \Lambda \cdot \mathbf{B}_0$

3 Selection of the hyperstatic forces

For each closed graph there are exactly $\alpha = M - O + 1$ independent cycles [26] that constitute a cycle basis, with M and O being the total number of members and the nodes of the graph, respectively. Denoting by M_{in} the members of the frame (with ground members not included), by O_{f} the foundation nodes, and by O_{in} the rest of the nodes of the frame, it is obvious that for the graph representation (Fig. 1) we have that $M = M_{\mathrm{in}} + O_{\mathrm{f}}$. On the other hand, we have that $O = O_{\mathrm{in}} + O_{\mathrm{f}} + 1$. Thus, one may write that $\alpha = M_{\mathrm{in}} - O_{\mathrm{in}}$.

There are 6α hyperstatic forces in a space frame. If one has a way to find a cycle basis, a statical basis may be found straightaway. The two-dimensional diagrammatic form of the space structure (Fig. 2) makes possible to use an algorithm that has been developed for the case of plane frames [22]. This algorithm utilizes a shortest path technique, from graph theory, to find the quickest way, going around the structure, between the two end nodes of a member, which is called the generator member. This path together with the generator member forms a cycle. The difficult task to select an independent cycle is simply done by increasing the “lengths” of the members of the cycle, which originally are set equal to *1*.

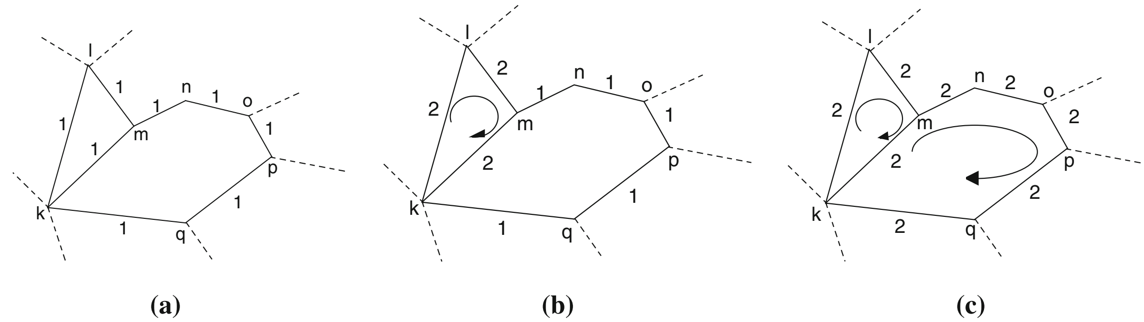

Fig. 5 Mesh base formation

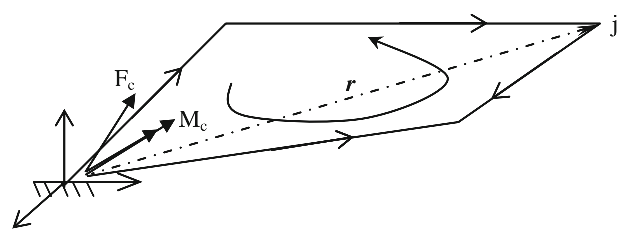

Fig. 6 Hyperstatic pair at each cycle

A cycle will enter the cycle basis if it satisfies the following admissibility rule:

$$(\text{length of the path}) < 2 \cdot \left[(\text{nodes along the path}) - 1\right]$$

If this rule is satisfied, the cycle enters the basis and the lengths of the members of the path become *2*.

The steps of the algorithm may be seen in Fig. 5, where a subgraph has been extracted from a main graph (Fig. 5a). Starting from the node *k* and selecting *km* as a generator member, the minimum path whose length is equal to *2* satisfies the admissibility rule and the cycle *klmk* enters the basis. The lengths of the members of the cycle then become equal to *2* (Fig. 5b). This cycle cannot be reselected because it will not pass the admissibility rule. Next, by picking up, for example *kq*, as a generator member the next obvious cycle enters the cycle basis (Fig. 5c).

There are cases of complicated graphs that this simple process may leave out some cycle [22], but there are remedies to overcome this problem. For such a case, it appears computationally more useful to use an alternative equivalent rule (this rule is employed in the present work), that is to add, to the length of the path, the length of the generator member. So the above rule may now be replaced by:

$$(\text{length of the cycle}) < 2 \cdot \left[(\text{nodes along the path})\right]$$

For the structure of Fig. 1, such a cycle basis may be seen in Fig. 2.

Starting with the nodes having the higher valency (number of members incident to a node) guarantees an almost minimal cycle basis in terms of the number of elements that constitute a cycle.

Each of the selected cycles may now be visualized as its real three-dimensional nature. In Fig. 6 one may see such a cycle. If we make a cut at any such cycle, a pair of resultant forces and moments $\mathbf{F}_\mathrm{c}$ and $\mathbf{M}_\mathrm{c}$ that constitute the hyperstatic forces for this cycle will appear. This pair may be analyzed in their components along the global axes x, y, z. Equilibrium with each of these components leads to stress resultants at each starting end j of the members that are met going around the perimeter of the cycle. More specifically, the opposites of these hyperstatic components are transferred to produce the corresponding forces and moments at the starting end j of each member of the cycle. The moments have to be augmented by the cross product of the components of the distance vector $\mathbf{r}$ from the cut to the end j (Fig. 6) with the hyperstatic force vector $\mathbf{F}_\mathrm{c}$. So one may write:

$$\begin{aligned} F_\mathrm{j}^{(m)} &= -F_\mathrm{c}^{(m)} \\ M_\mathrm{j}^{(m)} &= -M_\mathrm{c}^{(m)} - \left(\mathbf{r}_\mathrm{j} \times \mathbf{F}_\mathrm{c}\right)^{(m)} \end{aligned} \tag{8}$$

where m is equal to either x or y or z.

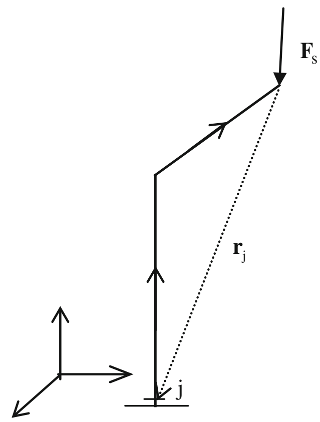

Fig. 7 Equilibrium with external load

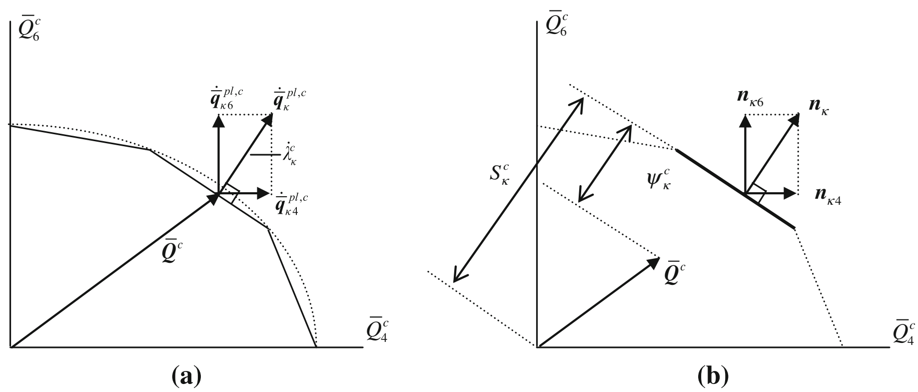

Fig. 8 **a** Linearized yield surface, **b** typical yield plane

If we provide unit values for the components of $\mathbf{F}_c$ and $\mathbf{M}_c$ the equilibrium matrix **B** may be established. It is obvious that if the specific member happens to be a part of another cycle too, the stress resultants for this member will be additive.

As far as equilibrium with the external loads is concerned, the shortest path technique is used to find the quickest way of each load to the ground in the form of 3D cantilevers (Fig. 1). Such a typical load path may be seen in Fig. 7. The forces and moments produced by the load vector components at the starting end j of each member along this path may be found in an analogous way as above:

$$F_{\mathrm{j}}^{(m)} = -F_{\mathrm{s}}^{(m)}$$
$$M_{\mathrm{j}}^{(m)} = -\left(\mathbf{r}_{\mathrm{j}} \times \mathbf{F}_{\mathrm{s}}\right)^{(m)} \tag{9}$$

For unit values for the components of $\mathbf{F}_s$, the entries to the matrix $\mathbf{B}_0$ may be found. It is obvious that if the specific member happens to be a part of other load paths, its stress resultants will be additive.

4 Problem formulation

We assume a perfectly plastic material. Plasticity is considered concentrated at the critical cross sections located at the member's end nodes. A "generalized plastic hinge" of zero length will appear whenever the combination of the components of the vector $\bar{\mathbf{Q}}^c$ at a cross section c touches the generally nonlinear plastic yield surface. An interaction between two components may be seen in Fig. 8.

The yield surface may then be linearized using planes to approximate it. The plastic strain vector is considered orthogonal to any of these planes and directed outward; the length of this vector on any such plane κ is denoted by $\dot{\lambda}_\kappa$. Thus, one may write for the plastic vector at a particular critical section c:

$$\dot{\mathbf{q}}_{\kappa}^{\mathrm{pl,c}} = \dot{\lambda}_{\kappa}^{\mathrm{c}} \cdot \mathbf{n}_{\kappa}, \quad \dot{\lambda}_{\kappa}^{\mathrm{c}} \geq 0 \tag{10}$$

where $\mathbf{n}_{\kappa}$ denotes the outward unit normal vector to the plane κ (Fig. 8b).

The sign convention of the components of the plastic vector follows the ones of the corresponding stress resultants.

Plastically admissible combinations of stress resultants are those for which the stress vector $\bar{\mathbf{Q}}^{\mathrm{c}}$ at a critical section lies within the yield surface. This may be expressed [27] through:

$$\mathbf{n}_{\kappa}^{\mathrm{T}} \cdot \bar{\mathbf{Q}}^{\mathrm{c}} + \Psi_{\kappa}^{\mathrm{c}} = \mathrm{S}_{\kappa}^{\mathrm{c}}, \quad \Psi_{\kappa}^{\mathrm{c}} \geq 0 \tag{11}$$

The complementary ways of the activation or not of the κth yield surface are given by the well-known complementarity condition:

$$\Psi_{\kappa}^{\mathrm{c}} \cdot \dot{\lambda}_{\kappa}^{\mathrm{c}} = 0 \tag{12}$$

If we group the terms $\mathbf{n}_{\kappa}$, S_{κ}, $\dot{\lambda}_{\kappa}$ in $\mathbf{N}$, $\mathbf{S}$, and $\dot{\boldsymbol{\lambda}}$, respectively, for all the possible planes at the critical sections of all the members of the frame, Eq. (7) after using the transformation (4), together with Eqs. (11) and (12), are the Karush–Kuhn–Tucker conditions of the plastic limit analysis [28]. These lead to the following force-based unsafe program which needs to be solved:

$$\begin{aligned} &\text{Minimize } \mathrm{s} = \mathbf{S}^{\mathrm{T}}\dot{\boldsymbol{\lambda}} \\ &\text{Subject to:} \\ &\begin{bmatrix} \mathbf{g}_0^{\mathrm{T}} \cdot \mathbf{T} \cdot \mathbf{N} \\ \mathbf{G}^{\mathrm{T}} \cdot \mathbf{T} \cdot \mathbf{N} \end{bmatrix} \dot{\boldsymbol{\lambda}} = \begin{bmatrix} 1 \\ \mathbf{0} \end{bmatrix} \\ &\ \dot{\boldsymbol{\lambda}} \geq \mathbf{0} \end{aligned} \tag{13}$$

where $\mathbf{N} = \begin{bmatrix} \mathbf{N}^1 & \dots & \mathbf{0} \\ \vdots & \ddots & \vdots \\ \mathbf{0} & \dots & \mathbf{N}^{\mathrm{ncs}} \end{bmatrix}$
with the dimensions being $(6 \cdot \mathrm{ncs}) \times (\mathrm{npl} \cdot \mathrm{ncs})$, where ncs denotes the number of the critical sections of the frame equal to $2 \cdot M_{\mathrm{in}}$, and npl the number of planes that each yield surface is linearized with; for a proper description $\mathrm{npl} \geq 8$.

Any standard LP algorithm, like the simplex technique or an interior-point algorithm [12], may be used to solve the linear program (13). Interior-point algorithms, which are particularly suited to solve sparse large-scale problems with linear or nonlinear constraints (e.g., [17,29]), are increasingly been employed in limit analysis problems, the last decade. In the present work both sparse solvers, one using the simplex algorithm and one using a LP interior-point algorithm, have been implemented. Both solvers are contained in the optimization package MOSEK [30].

5 Computational and programming considerations

Based on the duality of mathematical programming, four different limit analysis LP programs, in the framework of either the force or the displacement method, may be written. The variables of these LP programs may be either kinematic or static ones. Also, the number of constraints of the primal LP is equal to the number of variables of the dual LP.

The number of constraints of the kinematic program (13), for a space frame with no releases, is $m = 1 + 6 \cdot \alpha = 1 + 6 \cdot (M_{\mathrm{in}} - O_{\mathrm{in}})$, whereas the number of variables, with the variables being the lengths of the plastic vectors, is $n_{\mathrm{v}} = \mathrm{npl} \cdot \mathrm{ncs}$. On the other hand, the kinematic LP program that may be formulated using the alternative displacement method has $m' = 1 + 6 \cdot M_{\mathrm{in}}$ constraints and $n'_{\mathrm{v}} = \mathrm{npl} \cdot \mathrm{ncs} + 6 \cdot O_{\mathrm{in}}$ variables, with the extra terms being the independent displacements of the frame [27]. The size of the matrices involved (i.e., the number of constraints and the number of variables) is of course one parameter that influences the computing time. Thus, a force-based LP like the kinematic program (13), which has the fewer number of constraints and variables, is the more suitable to solve.

Additionally, the procedure of establishing a near-optimal cycle basis that was described above leads to hypersparse $\mathbf{G}$ matrices, which one should take into advantage, using sparse solvers [30].

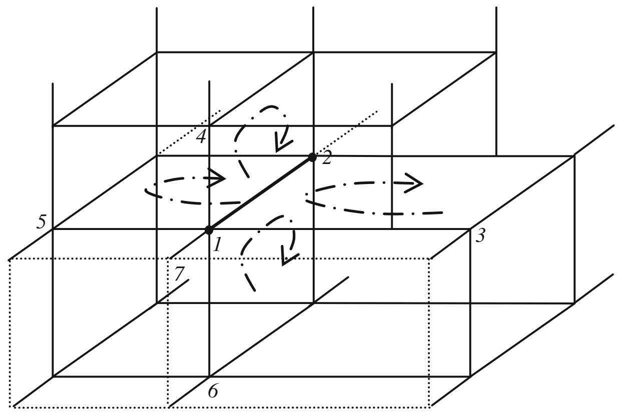

Fig. 9 Part of a general multistorey–multibay frame

The very sparse form of the equilibrium matrix **B** may be easily demonstrated in the one-storey configuration of Figs. 1, 2. We may see that there are, at mostly, two nonzero block entries rowise (Eq. 14).

$$\begin{Bmatrix} \mathbf{Q}_{N,p}^{(1)} \\ \mathbf{Q}_{N,p}^{(2)} \\ \mathbf{Q}_{N,p}^{(3)} \\ \mathbf{Q}_{N,p}^{(4)} \\ \mathbf{Q}_{N,p}^{(5)} \\ \mathbf{Q}_{N,p}^{(6)} \\ \mathbf{Q}_{N,p}^{(7)} \\ \mathbf{Q}_{N,p}^{(8)} \\ \mathbf{Q}_{N,p}^{(9)} \end{Bmatrix} = \begin{bmatrix} \mathbf{B}_1^{(1)} & \mathbf{B}_2^{(1)} & \mathbf{0} & \mathbf{0} \\ \mathbf{B}_1^{(2)} & \mathbf{0} & \mathbf{B}_3^{(2)} & \mathbf{0} \\ \mathbf{B}_1^{(3)} & \mathbf{0} & \mathbf{0} & \mathbf{B}_4^{(3)} \\ \mathbf{B}_1^{(4)} & \mathbf{0} & \mathbf{0} & \mathbf{B}_4^{(4)} \\ \mathbf{B}_1^{(5)} & \mathbf{0} & \mathbf{0} & \mathbf{0} \\ \mathbf{0} & \mathbf{B}_2^{(6)} & \mathbf{0} & \mathbf{0} \\ \mathbf{0} & \mathbf{B}_2^{(7)} & \mathbf{B}_3^{(7)} & \mathbf{0} \\ \mathbf{0} & \mathbf{0} & \mathbf{B}_3^{(8)} & \mathbf{B}_4^{(8)} \\ \mathbf{0} & \mathbf{0} & \mathbf{0} & \mathbf{B}_4^{(9)} \end{bmatrix} \cdot \begin{Bmatrix} \mathbf{p}_1 \\ \mathbf{p}_2 \\ \mathbf{p}_3 \\ \mathbf{p}_4 \end{Bmatrix} \tag{14}$$

$\mathbf{Q}_{N,p}^{(i)}$ is the 6×1 vector of the independent forces of the member i due to the indeterminacy of the frame, $\mathbf{p}_j$ is the 6×1 vector of hyperstatic forces of a topological cycle j, and $\mathbf{B}_j^{(i)}$ is the corresponding 6×6 block entry in the **B** matrix.

On the other hand, the equilibrium, in a displacement-based LP formulation, is expressed by equilibrating the forces, acting on a node, with the stress resultants of the members that are incident to this node [20]. Built in this way the equilibrium matrix becomes denser than above. This may be easily seen for the configuration of Fig. 1 where three nonzero 6×6 block entries would be needed rowise, since most of the nodes connect three members.

The same pattern difference between the two formulations holds for the most general case, shown in Fig. 9, where one may see a part of a frame that consists of several bays and storeys. It is easy now to visualize that as any member will belong to at most four cycles (a typical member with end nodes *1* and *2* is shown in the figure), the maximum number of entries in the equilibrium matrix for the force-based approach will be four nonzero 6×6 block entries rowise. At the same time, we see that the members connected to a typical node (node *1* in the figure) are six, which will require six nonzero block entries rowise if the equilibrium matrix were to be built in a displacement-based formulation.

Thus, the force-based formulation presented, combined with the solution of the kinematic program, is the most efficient, in terms of computing time, 3D frame limit analysis procedure that may be written.

A computer program that implements the theory described above was written in FORTRAN. The shortest path technique introduced by Nicholson [31] is used, whose coding may be found in the literature [32]. The Lagrange multipliers of the optimum solution provide values for the hyperstatic forces **p** from which using (7), a safe distribution of the stress resultants may be established.

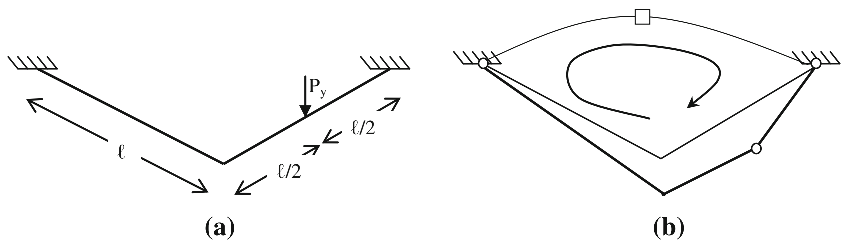

Fig. 10 **a** Geometry, **b** cycle basis and collapse mechanism

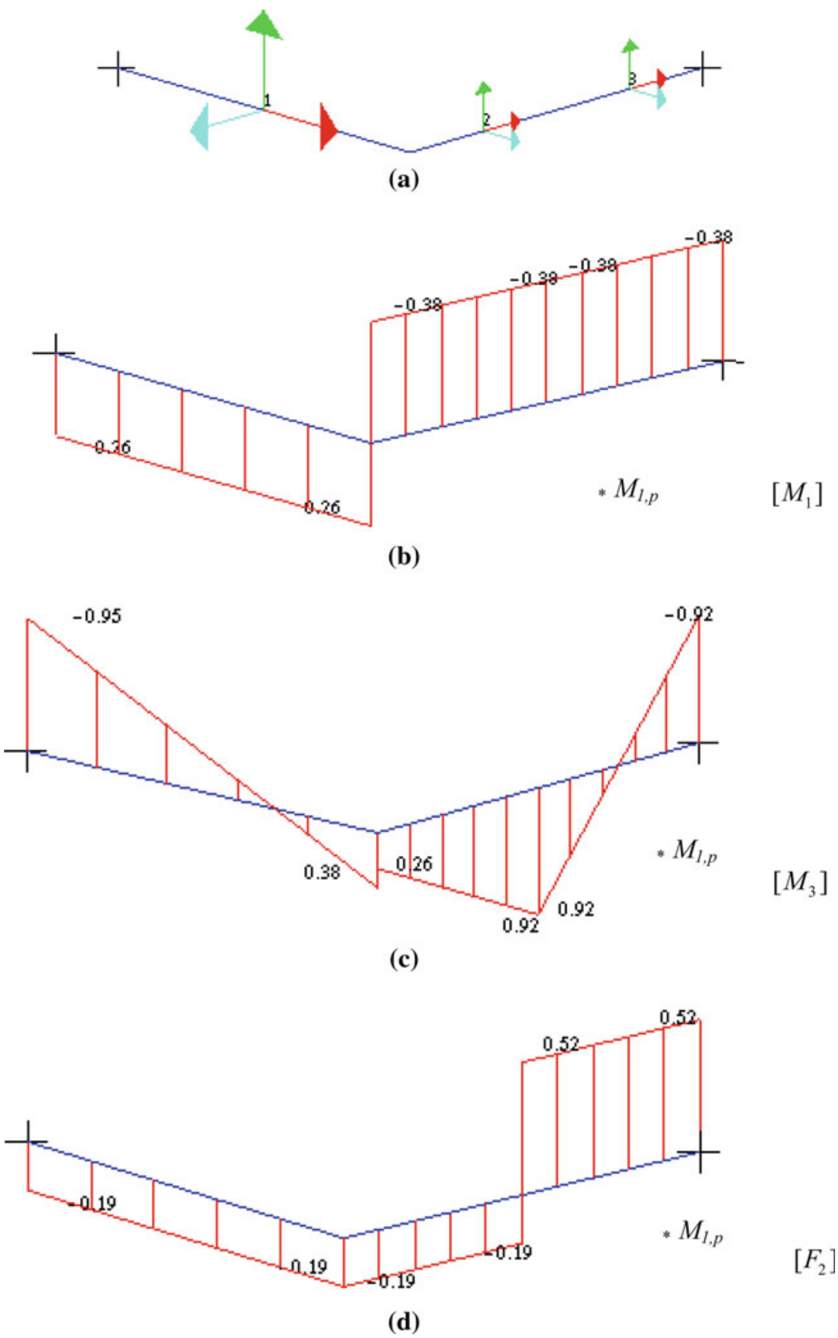

Fig. 11 Member numbering, local axes, and distributions of moments and shear force at collapse

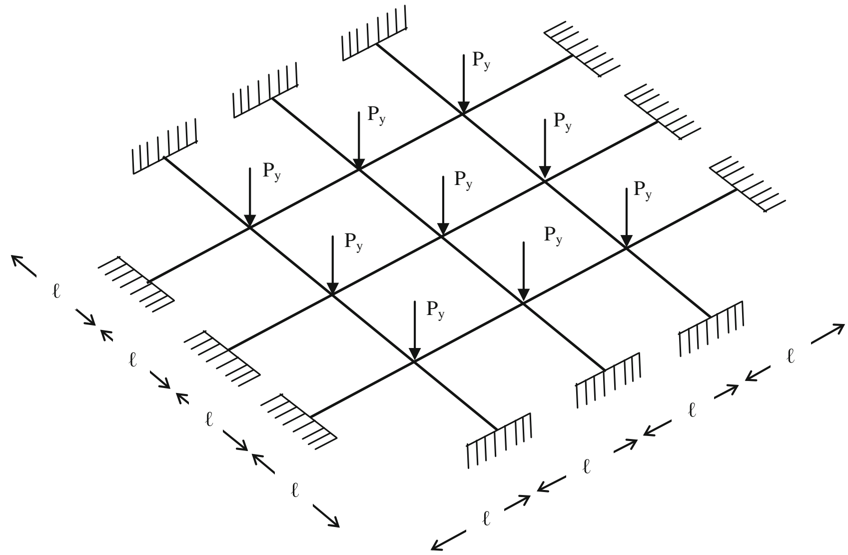

Fig. 12 Rectangular grillage

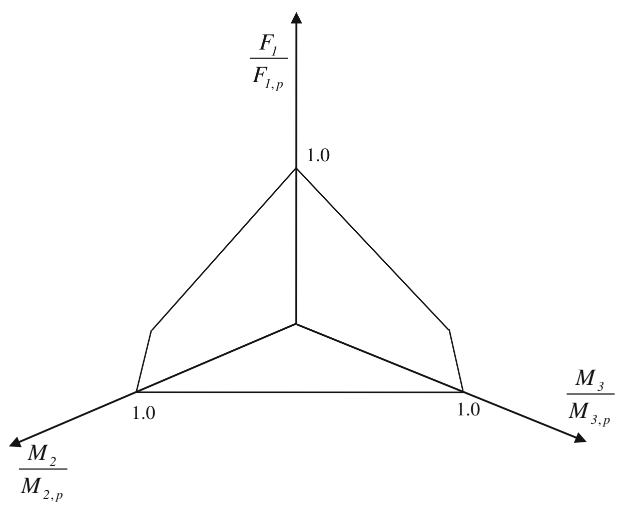

Fig. 13 Yield planes

6 Numerical examples

Examples of application of increasing complexity, using different yield surfaces, are presented next. The first three examples were chosen so as to indicate the robustness and the last one to mark also the computational efficiency of the proposed method. A pre- and post-processing graphics package that checks the data and may plot results was written as a companion to the limit analysis computer program.

6.1 Limit analysis of grillages

A grillage constitutes a special type of a space frame in which all the members of the frame lie in one plane and all loads act perpendicular to that plane. To establish equilibrium equations for such structures, it suffices to take moments about axes lying in the plane.

Such a member, therefore, is under the action of combined bending and torsion. If the influence of the transverse shear on the formation of a plastic hinge is disregarded, the yield condition involves only twisting and bending moment acting at a typical cross section of the frame.

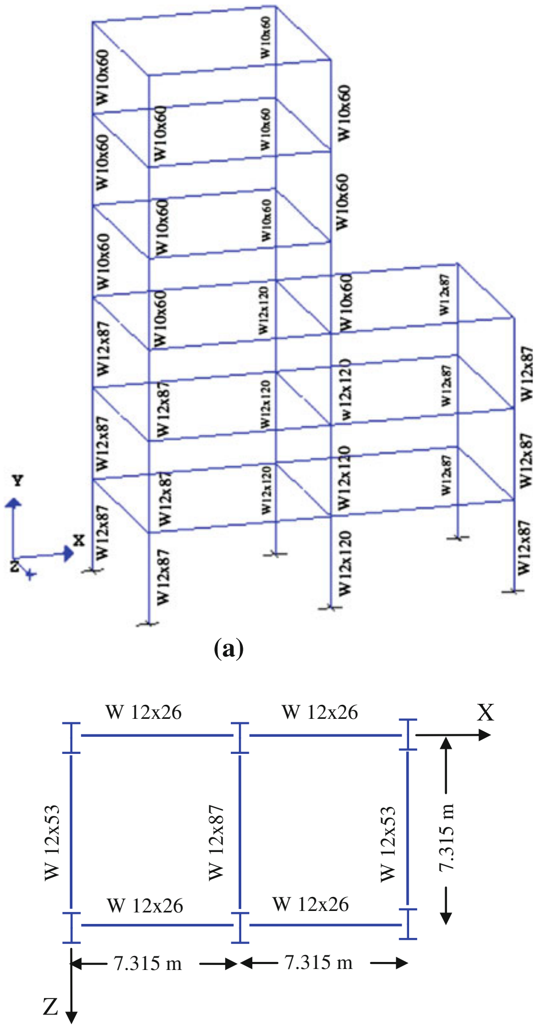

Fig. 14 Six-storey building: **a** perspective view, **b** plan view

Table 1 Plastic capacities for the six-storey building

Section	$F_{1,p}$ (KN)	$M_{2,p}$ (KNm)	$M_{3,p}$ (KNm)
W12 × 87	4,125.00	247.45	540.75
W12 × 120	5,700.00	349.75	762.00
W12 × 53	2,525.00	119.25	319.25
W12 × 26	1,235.00	33.48	152.40
W10 × 60	2,850.00	143.38	305.50

If the plastic moment capacity in the absence of twisting moment is $M_{3,\text{p}}$ and the plastic twisting moment capacity in the absence of bending is $M_{1,\text{p}}$, then for many structural members that are used in practice, for example, tubes of circular or rectangular section, the yield criteria may be approximated by a circle:

$$\left(M_1/M_{1,\text{p}}\right)^2 + \left(M_3/M_{3,\text{p}}\right)^2 = 1 \tag{15}$$

Sixteen planes, four for each quadrant, may be used to inscribe this circle. Supposing further, for the case of simplicity, that $M_{1,\text{p}} = M_{3,\text{p}}$, it turns out that S_κ is constant and approximately equal to *1* for all the planes whereas the normal $\boldsymbol{n}_\kappa$, for each plane, forms an angle ϑ_κ with respect to the horizontal axis given by (16):

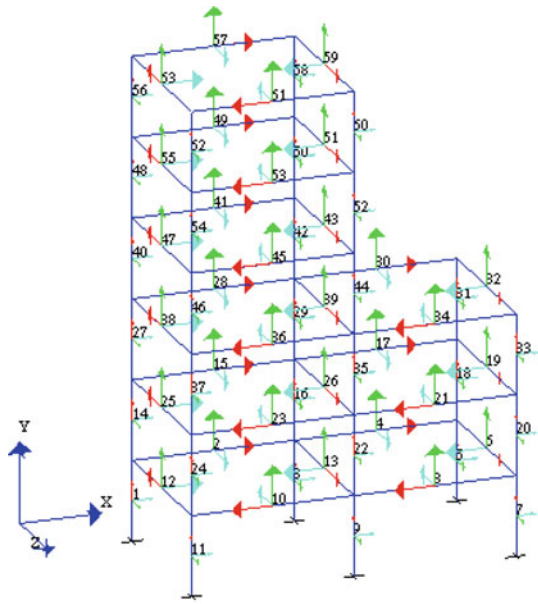

(a)

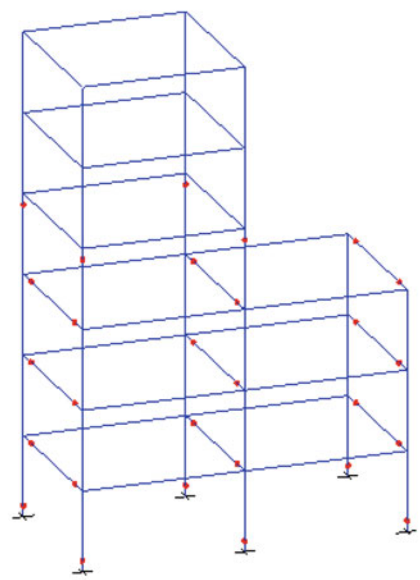

(b)

Fig. 15 **a** Member numbering and local axes. **b** Distribution of plastic hinges in collapse mechanism

$$\vartheta_\kappa = \frac{\pi}{16} + (\kappa - 1) \cdot \frac{\pi}{8}, \quad \kappa\text{=1,2,...,16} \tag{16}$$

Equation (16) may be used to form the (6×16) $\mathbf{N}^c$ matrix for each critical cross section c:

$$\mathbf{N}^c = \begin{bmatrix} 0 & 0 & \cdots\cdots & 0 \\ 0 & 0 & \cdots\cdots & 0 \\ 0 & 0 & \cdots\cdots & 0 \\ \cos\vartheta_1 & \cos\vartheta_2 & \cdots\cdots & \cos\vartheta_{16} \\ 0 & 0 & \cdots\cdots & 0 \\ \sin\vartheta_1 & \sin\vartheta_2 & \cdots\cdots & \sin\vartheta_{16} \end{bmatrix}, \quad c = 1, 2, \ldots, \text{ncs} \tag{17}$$

Table 2 Safe force and moment distribution for the six-storey building at collapse

Member no.	Critical sect.	F_1	F_2	F_3	M_1	M_2	M_3
1	1	−586.96	225.02	−22.69	8.38	0	502.28
	2	−586.96	225.02	−22.69	8.38	83.02	−320.86
2	3	35.72	−41.07	0	−45.49	0	−150.2
	4	35.72	−41.07	0	−45.49	0	150.2
3	5	−869.99	314.28	−32.38	−115.58	0	703.85
	6	−869.99	314.28	−32.38	−115.58	118.44	−445.8
4	7	15.86	41.4	0	−337.94	0	151.42
	8	15.86	41.4	0	−337.94	0	−151.42
5	9	−385.42	158.84	55.07	9.38	0	515.49
	10	−385.42	158.84	55.07	9.38	−201.46	−65.53
6	11	0	87.29	0	251.3	0	319.25
	12	0	87.29	0	251.3	0	−319.25
7	13	−915.16	62.6	3.6	0	0	473.38
	14	−915.16	62.6	3.6	0	−13.15	244.4
8	15	0	−41.67	0	−307.74	0	−152.4
	16	0	−41.67	0	−307.74	0	152.4
9	17	−1823.23	150.33	−3.6	294.01	0	583.05
	18	−1823.23	150.33	−3.6	294.01	13.15	33.15
10	19	11.26	41.48	0	−408.26	0	151.71
	20	11.26	41.48	0	−408.26	0	−151.71
11	21	−1772.48	189.69	0	0.37	0	346.94
	22	−1772.48	189.69	0	0.37	0	−346.94
12	23	0	−87.29	0	−146.49	0	−319.25
	24	0	−87.29	0	−146.49	0	319.25
13	25	0	147.85	0	−65.32	0	540.75
	26	0	147.85	0	−65.32	0	−540.75
14	27	−456.7	151.64	−58.41	8.38	−213.67	43.88
	28	−456.7	151.64	−58.41	8.38	0	−510.82
15	29	35.72	−41.07	0	−191.57	0	−150.2
	30	35.72	−41.07	0	−191.57	0	150.2
16	31	−747.34	240.9	−12.53	−115.58	54.35	387.4
	32	−747.34	240.9	−12.53	−115.58	100.17	−493.81
17	33	28.1	41.19	0	−37.13	0	150.67
	34	28.1	41.19	0	−37.13	0	−150.67
18	35	−254.82	85.45	70.94	9.38	201.26	−84.23
	36	−254.82	85.45	70.94	9.38	−58.22	−396.81
19	37	0	87.29	0	98.79	0	319.25
	38	0	87.29	0	98.79	0	−319.25
20	39	−609.72	62.6	3.6	0	−112.06	255.91
	40	−609.72	62.6	3.6	0	−125.21	26.93
21	41	0	−41.67	0	18.15	0	−152.4
	42	0	−41.67	0	18.15	0	152.4
22	43	−1405.57	150.33	7.67	294.01	79.17	473.38
	44	−1405.57	150.33	7.67	294.01	51.12	−76.52
23	45	11.26	41.48	0	−369.3	0	151.71
	46	11.26	41.48	0	−369.3	0	−151.71
24	47	−1467.24	189.69	−11.26	0.37	−5.21	380.57
	48	−1467.24	189.69	−11.26	0.37	35.99	−313.32
25	49	0	−87.29	0	−87.46	0	−319.25
	50	0	−87.29	0	−87.46	0	319.25
26	51	0	147.85	0	−118.59	0	540.75
	52	0	147.85	0	−118.59	0	−540.75
27	53	−326.44	78.26	−94.13	8.38	−237.66	0
	54	−326.44	78.26	−94.13	8.38	106.66	−286.26
28	55	−66.7	−35.33	−1.15	88.58	−8.38	−110.12
	56	−66.7	−35.33	−1.15	88.58	0	148.28
29	57	−624.49	167.51	−4.91	−115.58	−17.94	−107.49
	58	−624.49	167.51	−4.91	−115.58	0	−720.26
30	59	−99.03	34.16	−1.28	−156.46	0	146.29
	60	−99.03	34.16	−1.28	−156.46	9.38	−103.61
31	61	−124.44	12.07	99.03	9.38	191.23	−114.69
	62	−124.44	12.07	99.03	9.38	−171.03	−158.84
32	63	−62.6	86.2	0	67.42	0	315.29
	64	−62.6	86.2	0	67.42	0	−315.29

Table 2 Continued

Member no.	Critical sect.	F_1	F_2	F_3	M_1	M_2	M_3
33	65	−304.29	62.6	3.6	0	−71.6	364.33
	66	−304.29	62.6	3.6	0	−84.76	135.35
34	67	−3.6	−41.61	0	−450.64	0	−152.18
	68	−3.6	−41.61	0	−450.64	0	152.18
35	69	−987.91	150.33	18.93	294.01	170.4	76.78
	70	−987.91	150.33	18.93	294.01	101.16	−473.12
36	71	−22.53	41.29	0	−243.32	0	151.01
	72	−22.53	41.29	0	−243.32	0	−151.01
37	73	−1162	189.69	−22.53	0.37	−28.26	375.23
	74	−1162	189.69	−22.53	0.37	54.14	−318.66
38	75	−58.35	−86.28	0	−96.87	0	−315.56
	76	−58.35	−86.28	0	−96.87	0	315.56
39	77	0	147.85	0	102.32	0	540.75
	78	0	147.85	0	102.32	0	−540.75
40	79	−200.92	64.37	−27.43	0	−100.33	−59.28
	80	−200.92	64.37	−27.43	0	0	−294.73
41	81	−27.43	22.9	−4.02	−193.21	0	150.71
	82	−27.43	22.9	−4.02	−193.21	29.41	−16.83
42	83	−488.87	94.27	27.43	−115.58	100.33	65.53
	84	−488.87	94.27	27.43	−115.58	0	−279.3
43	85	0	73.11	−5.29	−2.82	0	319.25
	86	0	73.11	−5.29	−2.82	38.73	−215.57
44	87	−570	150.33	0	294.01	0	274.95
	88	−570	150.33	0	294.01	0	−274.95
45	89	0	20.83	−4.58	340.59	−33.48	0
	90	0	20.83	−4.58	340.59	0	−152.4
46	91	−857.95	131.34	0	0.37	0	240.23
	92	−857.95	131.34	0	0.37	0	−240.23
47	93	−143.61	−84.8	0	−150.71	0	−310.17
	94	−143.61	−84.8	0	−150.71	0	310.17
48	95	−132.15	138.62	0	0	0	208.65
	96	−132.15	138.62	0	0	0	−298.42
49	97	0	20.83	−4.58	−81.45	0	152.4
	98	0	20.83	−4.58	−81.45	33.48	0
50	99	−362.6	16.86	−5.29	−144.99	14.02	−153.25
	100	−362.6	16.86	−5.29	−144.99	33.38	−214.94
51	101	−47.92	4.75	1.78	−33.38	118.12	0
	102	−47.92	4.75	1.78	−33.38	105.13	−34.78
52	103	−341.24	145.75	5.29	221.81	2.82	281.21
	104	−341.24	145.75	5.29	221.81	−16.55	−251.95
53	105	0	27.7	−3.07	367.02	−22.44	50.25
	106	0	27.7	−3.07	367.02	0	−152.4
54	107	−575.84	−7.7	0	0.37	−1.69	−270.64
	108	−575.84	−7.7	0	0.37	−1.69	−242.49
55	109	0	−87.29	0	−154.09	0	−319.25
	110	0	−87.29	0	−154.09	0	319.25
56	111	−63.79	69.81	0	0	−1.69	102.28
	112	−63.79	69.81	0	0	−1.69	−153.08
57	113	0	25.4	−3.57	166.17	0	152.4
	114	0	25.4	−3.57	166.17	26.14	−33.42
58	115	−170.04	−13.18	−3.52	−60.36	0	−296.39
	116	−170.04	−13.18	−3.52	−60.36	12.87	−248.16
59	117	−90.14	31.84	3.52	−46.29	86.49	82
	118	−90.14	31.84	3.52	−46.29	60.76	−150.89
60	119	−187.71	94.77	3.52	94.24	−33.42	149.85
	120	−187.71	94.77	3.52	94.24	−46.29	−196.81
61	121	0	20.6	−4.63	45.92	−33.48	0
	122	0	20.6	−4.63	45.92	0.37	−150.71
62	123	−284.37	−4.63	0	0.37	0	−290.26
	124	−284.37	−4.63	0	0.37	0	−273.33
63	125	0	−87.29	0	−150.71	0	−319.25
	126	0	−87.29	0	−150.71	0	319.25

6.1.1 Right-angle bent frame

To test the software written, as a first example of application, the unsymmetrical right-angle bent (Fig. 10a) is solved. In Fig. 10b one may see the unique cycle identified by the computer program together with the collapse mechanism. This mechanism is the same over-complete mechanism as it was also pointed out by Heyman [33], who solved this problem analytically. The collapse load factor comes out to be $P_y^{\mathrm{c}} = 0.7109 M_{1,\mathrm{p}}$, which is almost identical to the one analytically computed [33]: $P_y^{\mathrm{c}} = \frac{16}{\sqrt{10}} \cdot \frac{M_{1,\mathrm{p}}}{\ell} == 0.7155 M_{1,\mathrm{p}}$

In Fig. 11 one may see the evaluated, by the program, distributions of the various stress resultants. To be able to determine also their directions, the local axes of the members are also plotted.

6.1.2 Rectangular grillage

The rectangular grillage shown in Fig. 12 is the next example of grillage type of problems. This example has been analytically solved by Chakrabarty [34]. The computed load factor turns out to be $P_y^{\mathrm{c}} = 2.30 M_{1,\mathrm{p}}/\ell$ which compares very well to the analytically evaluated $P_y^{\mathrm{c}} = 2.33 M_{1,\mathrm{p}}/\ell$.

6.2 Limit analysis of space frames under biaxial bending and axial force

Next, examples concerning 3D steel frames using the AISC [35] interaction surfaces for compact wide-flange sections are examined. For a specific cross section c, these may be expressed through the following equations:

$$\begin{array}{ll} \alpha_1^{\mathrm{c}} \cdot |F_1| + \alpha_2^{\mathrm{c}} \cdot |M_2| + \alpha_3^{\mathrm{c}} \cdot |M_3| = S_0^{\mathrm{c}} & \text{for } |F_1|/F_{1,\mathrm{p}}^{\mathrm{c}} \geq 0.2 \\ \alpha_4^{\mathrm{c}} \cdot |F_1| + \alpha_5^{\mathrm{c}} \cdot |M_2| + \alpha_6^{\mathrm{c}} \cdot |M_3| = S_0^{\mathrm{c}} & \text{for } |F_1|/F_{1,\mathrm{p}}^{\mathrm{c}} < 0.2 \end{array} \tag{18}$$

where $\alpha_1^{\mathrm{c}} = \frac{S_0^{\mathrm{c}}}{F_{1,\mathrm{p}}^{\mathrm{c}}}, \alpha_2^{\mathrm{c}} = \frac{8S_0^{\mathrm{c}}}{9M_{2,\mathrm{p}}^{\mathrm{c}}}, \alpha_3^{\mathrm{c}} = \frac{8S_0^{\mathrm{c}}}{9M_{3,\mathrm{p}}^{\mathrm{c}}}, \alpha_4^{\mathrm{c}} = \frac{S_0^{\mathrm{c}}}{2F_{1,\mathrm{p}}^{\mathrm{c}}}, \alpha_5^{i} = \frac{S_0^{\mathrm{c}}}{M_{2,\mathrm{p}}^{\mathrm{c}}}, \alpha_6^{\mathrm{c}} = \frac{S_0^{\mathrm{c}}}{M_{3,\mathrm{p}}^{\mathrm{c}}}$

with $F_{1,\mathrm{p}}^{\mathrm{c}}$, $M_{2,\mathrm{p}}^{\mathrm{c}}$, $M_{3,\mathrm{p}}^{\mathrm{c}}$ being the corresponding plastic capacities of the axial force and of the bending moments of the cross section, respectively, whereas S_0^{c} is its yield stress.

If one expands (18), we turn up with sixteen equations each one of which corresponds to the equation of a plane. If we plot these equations in a three-dimensional space, with the axes being the normalized axial force and the normalized bending moments, we can distinguish four quadrants for either a positive or a negative axial force. Two planes may be drawn for each quadrant that are represented by either the first or the second of the equations (18). Two such planes in the first quadrant for positive values of the stress resultants may be seen in Fig. 13.

Assuming S_0^{c} to be equal to S_κ^{c}, which is the distance of the origin of the axes (Fig. 8), equation (18) is the Hessian normal form of the equation of a plane and thus the various triads $(\pm)\alpha_l^{\mathrm{c}}, l = 1, \ldots, 3$ or $(\pm)\alpha_l^{\mathrm{c}}, l = 4, \ldots, 6$ play the role of the components of the unit normal vector to the plane κ. Thus, the (6×16) $\mathbf{N}^{\mathrm{c}}$ matrix for each cross section c will now look like:

$$\mathbf{N}^{\mathrm{c}} = \begin{bmatrix} \alpha_1^{\mathrm{c}} & \alpha_1^{\mathrm{c}} & \alpha_1^{\mathrm{c}} & -\alpha_1^{\mathrm{c}} & -\alpha_1^{\mathrm{c}} & -\alpha_1^{\mathrm{c}} & \alpha_1^{\mathrm{c}} & -\alpha_1^{\mathrm{c}} & \alpha_4^{\mathrm{c}} & \alpha_4^{\mathrm{c}} & \alpha_4^{\mathrm{c}} & -\alpha_4^{\mathrm{c}} & -\alpha_4^{\mathrm{c}} & -\alpha_4^{\mathrm{c}} & \alpha_4^{\mathrm{c}} & -\alpha_4^{\mathrm{c}} \\ 0 & 0 & 0 & 0 & 0 & 0 & 0 & 0 & 0 & 0 & 0 & 0 & 0 & 0 & 0 & 0 \\ 0 & 0 & 0 & 0 & 0 & 0 & 0 & 0 & 0 & 0 & 0 & 0 & 0 & 0 & 0 & 0 \\ 0 & 0 & 0 & 0 & 0 & 0 & 0 & 0 & 0 & 0 & 0 & 0 & 0 & 0 & 0 & 0 \\ -\alpha_2^{\mathrm{c}} & \alpha_2^{\mathrm{c}} & \alpha_2^{\mathrm{c}} & \alpha_2^{\mathrm{c}} & -\alpha_2^{\mathrm{c}} & -\alpha_2^{\mathrm{c}} & -\alpha_2^{\mathrm{c}} & \alpha_2^{\mathrm{c}} & -\alpha_5^{\mathrm{c}} & \alpha_5^{\mathrm{c}} & \alpha_5^{\mathrm{c}} & \alpha_5^{\mathrm{c}} & -\alpha_5^{\mathrm{c}} & -\alpha_5^{\mathrm{c}} & -\alpha_5^{\mathrm{c}} & \alpha_5^{\mathrm{c}} \\ -\alpha_3^{\mathrm{c}} & -\alpha_3^{\mathrm{c}} & \alpha_3^{\mathrm{c}} & \alpha_3^{\mathrm{c}} & \alpha_3^{\mathrm{c}} & -\alpha_3^{\mathrm{c}} & \alpha_3^{\mathrm{c}} & -\alpha_3^{\mathrm{c}} & -\alpha_6^{\mathrm{c}} & -\alpha_6^{\mathrm{c}} & \alpha_6^{\mathrm{c}} & \alpha_6^{\mathrm{c}} & \alpha_6^{\mathrm{c}} & -\alpha_6^{\mathrm{c}} & \alpha_6^{\mathrm{c}} & -\alpha_6^{\mathrm{c}} \end{bmatrix}$$

6.2.1 Six-storey building

The six-storey frame of Fig. 14, which was considered in [15], offers a first example. The yield strength of all the members is equal to 250 MPa. For the various members of the frame, AISC [35] sections were used, whose plastic capacities may be seen in Table 1.

The structure is subjected to both horizontal and vertical loads that vary proportionally. Wind loads along the z direction represent the horizontal loading. These loads were simulated as point loads applied at every beam to column joint having a value of 26.70 KN.

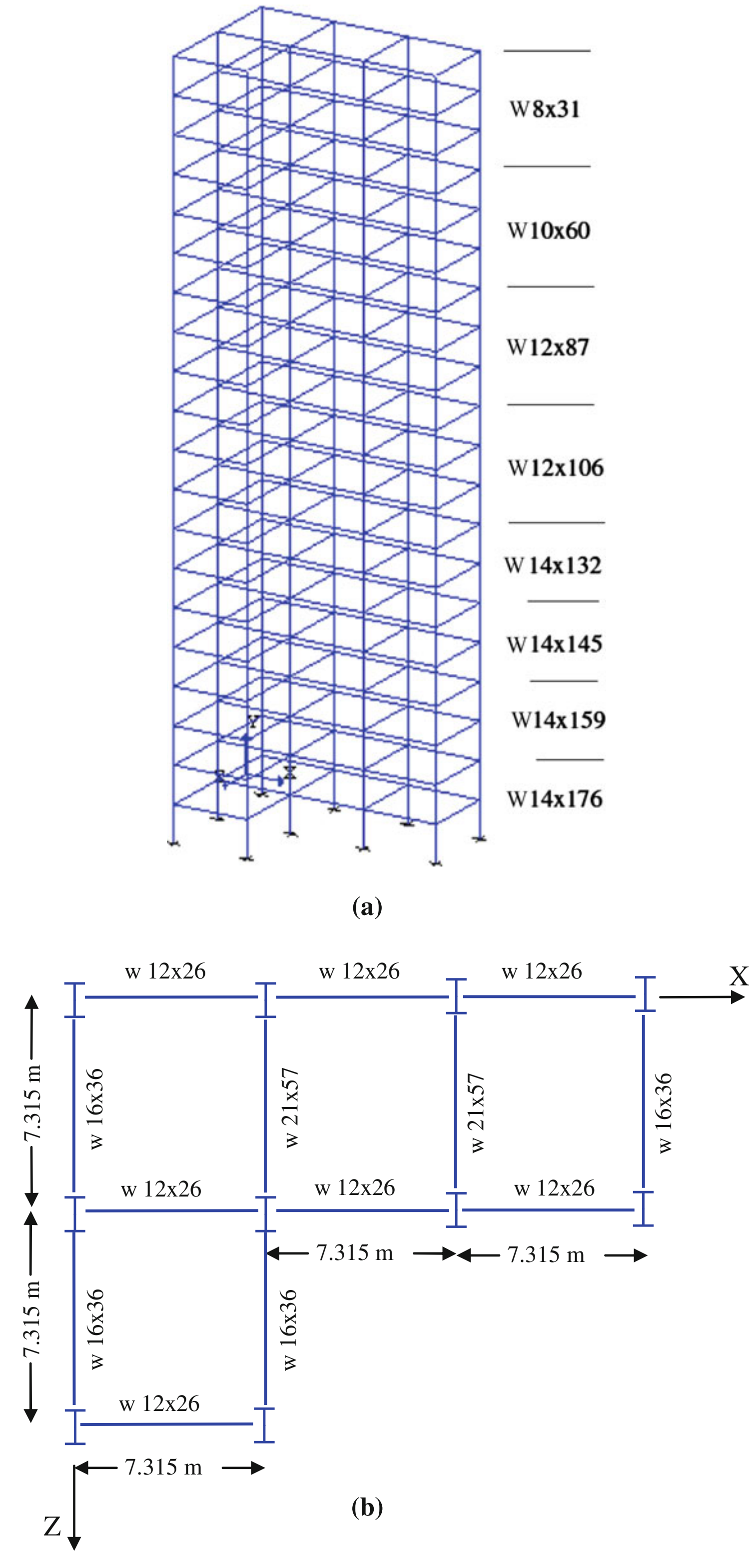

Fig. 16 Twenty-storey building: **a** perspective view, **b** plan view

Table 3 Plastic capacities for the six-storey building

Section	$F_{1,p}$ (KN)	$M_{2,p}$ (KNm)	$M_{3,p}$ (KNm)
W12 × 26	1, 701.59	46.17	210.19
W14 × 176	11, 516.32	920.96	1, 808.13
W16 × 36	2, 377.02	61.03	361.70
W21 × 57	3, 723.84	83.61	728.91
W14 × 159	10, 378.48	825.11	1, 621.59
W14 × 145	9, 482.00	751.32	1, 469.19
W14 × 132	8, 620.00	638.57	1, 322.31
W12 × 106	6, 930.48	424.45	926.48
W12 × 87	5, 689.20	341.28	745.80
W10 × 60	3, 930.72	197.74	421.35
W8 × 31	2, 030.87	79.68	171.78

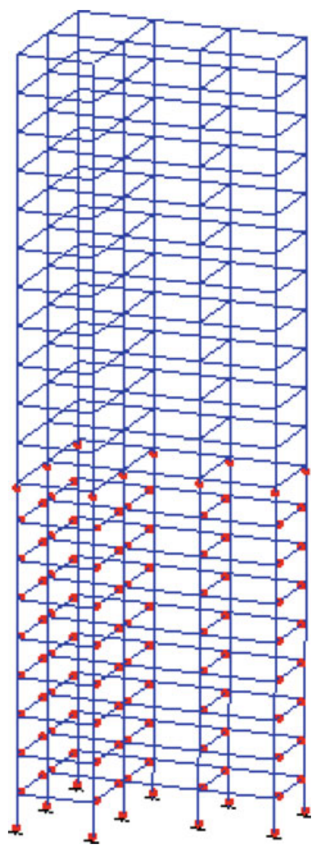

Fig. 17 Distribution of plastic hinges in the collapse mechanism

A uniform floor pressure of a value of 4.8 KN/m^2 was considered as a vertical loading. This loading is equivalent to a total load on each floor beam of the value of $P = 64.21$ KN. This load is then considered lumped at the two end nodes of the beam acting along the negative y direction and having the value of $P/2$. The collapse load factor turns out to be 2.75, which is roughly 10 % different from the predicted value in [15]. The collapse mechanism, consisted of twenty-eight plastic hinges (Fig. 15b), is obviously a sway type mechanism. One may see in Table 2 the evaluated safe stress resultants' distribution at collapse.

6.2.2 Twenty-storey building

The last example of application is also considered in [15] and is a relatively large building consisted of twenty storeys, whose geometric data can be seen in Fig. 16. The yield strength of all the members is taken equal to 344.8 MPa. The plastic capacities of the cross sections [35] are reported in Table 3.

A uniform floor pressure of 4.8 KN/m^2 was considered as lumped vertical loads, like in the previous example. Another loading was wind pressure of 0.96 kN/m^2 acting at the backside face along the z direction. The areas of the surrounding panels of a node served as a means to distribute this pressure evenly as equivalent nodal load. The load collapse factor obtained was 1.715, which is almost identical with the result obtained by [15]. One may observe a pure sway type of 116 plastic hinges collapse mechanism of the bottom nine floors (Fig. 17).

The computer program was run at a desktop computer with an Intel Core i7 at 3.20 GHz CPU with 6 GB RAM. The same, more or less, computing time was spent for the solution with either the sparse interior point or the sparse simplex solver of [30].

The result was obtained in just 2.15 s. This indicates the hypersparcity of the matrices involved, as from the 23×10^6 elements, only 13,800 are nonzero, that is, a reduction of 99.4 %.

7 Concluding remarks

A novel direct method for the limit analysis of elastoplastic space frames is presented. The method is based on linear programming and the unsafe theorem of plasticity and uses as a framework the force method. The implementation of the force method, using concepts from the theory of graphs like a cycle basis and the minimum path between two points of a directed graph, offers computational advantages over a displacement-based alternative, which is used almost exclusively at present.

It is believed that the presented approach is not difficult to follow and relatively easy to program. Thus, the method may become a useful tool for the practicing engineer, who would like to have a quick estimate of the strength of a three-dimensional skeletal structure.

Obviously, the method may also be employed for the shakedown analysis of such structures.

References

1. Orbison, J.G., McGuire, W., Abel, J.F.: Yield surface applications in nonlinear steel frame analysis. Comp. Methods Appl. Mech. Eng. **33**, 557–573 (1982)
2. Liew, J.Y.R., Chen, H., Shanmugan, N.E., Chen, W.F.: Improved nonlinear plastic hinge analysis of space frame structures. Eng. Struct. **22**, 1324–1338 (2000)
3. Kim, S-E., Park, M-H., Choi, S-H.: Direct design of three-dimensional frames using practical advanced analysis. Eng. Struct. **23**, 1491–1502 (2001)
4. Long, H.V., Nguyen, D.H.: Second-order plastic-hinge analysis of 3-D steel frames including strain hardening effects. Eng. Struct. **30**, 3505–3512 (2008)
5. Neal, B.G.: The Plastic Method of Structural Analysis. Chapman & Hall, London (1970)
6. Cohn, M.Z., Ghosh, S.K., Parimi, S.R.: Unified approach to theory of plastic structures. Eng. Mech. (ASCE) **98**, 1133–1158 (1972)
7. Maier, G., Pastor, J., Ponter, A.R.S., Weichert, D.: Direct methods of limit and shakedown analysis. In: de Borst, R., Mang, H.A. (eds.) Comprehensive Structural Integrity—Fracture of Materials from Nano to Macro, : Numerical and Computational Methods, vol. 3, pp 637–684. Elsevier (2003)
8. Dantzig, G.: Linear Programming and Extensions. Princeton University Press, Princeton (1963)
9. Karmarkar, N.: A new polynomial time algorithm for linear programming. Combinatorica **4**(4), 373–395 (1984)
10. Andersen, K.D., Christiansen, E., Overton, M.L.: Computing limit loads by minimizing a sum of norms. SIAM J. Sci. Comp. **3**, 1046–1062 (1998)
11. Pastor, F., Loute, E.: Solving limit analysis problems: an interior point method. Commun. Numer. Methods Eng. **21**, 631–642 (2005)
12. Vanderbei, R.J.: Linear Programming: Foundations and Extensions. 3rd edn. Kluwer, Dordrecht (2008)
13. Weichert, D., Ponter, A.R.S. (eds.): Limit States of Materials and Structures. Springer, Wien (2009)
14. Nguyen, D.H.: CEPAO—an automatic program for rigid-plastic and elastic-plastic analysis and optimization of frame structures. Eng. Struct. **6**, 33–51 (1984)
15. Long, H.V., Nguyen, D.H.: Limit and shakedown analysis of 3-D Steel frames. Eng. Struct. **30**, 1895–2004 (2007)
16. Long, H.V., Nguyen, D.H.: Plastic optimization of 3D steel frames under fixed or repeated loading: reduction formulation. Eng. Struct. **32**, 1092–1099 (2010)
17. Skordeli, M-AA., Bisbos, C.D.: Limit and shakedown analysis of 3d steel frames via approximate ellipsoidal yield surfaces. Eng. Struct. **32**, 1556–1557 (2010)
18. SAP2000 V-14.2.4. Integrated Finite Element Analysis and Design of Structures-Basic Analysis Reference Manual. Computers and Structures Inc, Berkeley (2010)
19. Kaneko, I., Lawo, M., Thierauf, G.: On computational procedures for the force method. Int. J. Numer. Methods. Eng. **18**, 1469–1495 (1982)
20. Damkilde, L., Høyer, O.: An efficient implementation of limit state calculations based on lower-bound solutions. Comput. Struct **49**(6), 953–962 (1993)

21. Kaveh, A., Koohestani, K.: An efficient graph-theoretical force method for three-dimensional finite element analysis. Commun. Numer. Methods Eng. **24**, 1533–1551 (2008)
22. Spiliopoulos, K.V.: On the automation of the force method in the optimal plastic design of frames. Comp. Methods Appl. Mech. Eng. **141**, 141–156 (1997)
23. Spiliopoulos, K.V.: A fully automatic force method for the optimal shakedown design of frames. Comp. Mech. **23**(4), 299–307 (1999)
24. Spiliopoulos, K.V., Patsios, T.N.: A quick estimate of the strength of uniaxially tied framed structures. J. Constr. Steel Res. **65**, 1763–1775 (2009)
25. de Henderson, J.C., Maunder, E.A.W.: A problem in applied topology: on the selection of cycles for the flexibility analysis of skeletal structures. J. Inst. Maths. Appl. **5**, 254–269 (1969)
26. de Henderson, J.C., Bickley, W.G.: Statical indeterminacy of a structure. J. Aircr Eng. **27**, 400–402 (1955)
27. Smith, D.L.: Plastic limit analysis. In: Smith DL (ed.) Mathematical Programming Methods in Structural Plasticity. pp. 61–82, Springer, Berlin (1990)
28. Maier, G.: Linear flow-laws of elastoplasticity: a unified general approach. Rendic. Acad. Naz. Lincei, Series 8, **47**, 266 (1969)
29. Trillat, M., Pastor, J.: Limit analysis and Gurson's model. Eur. J. Mech. Solids **24**, 800–819 (2005)
30. MOSEK ApS, Denmark.: the MOSEK optimization tools version 6.0 (revision 135)—user's manual and reference (2012) Download at http://www.mosek.com
31. Nicholson, T.A.J.: Finding the shortest route between two points in a network. Comput. J. **26**, 275–280 (1966)
32. Lau, H.T.: Algorithms on Graphs. Tab Books (1989)
33. Heyman, J.: Elements of the Theory of Structures. Cambridge University Press, Cambridge (1996)
34. Chakrabarty, J.: Theory of Plasticity. Elsevier Butterworth-Heinemann, Oxford (2006)
35. AISC.: Load and Resistance Factor Design Specification for Steel Buildings. American Institute of Steel Construction, Chicago (1993)